Journal of Materials Chemistry A

PAPER

View Article Online
View Journal | View Issue

Cite this: J. Mater. Chem. A, 2016, 4, 1708

PBDT-TSR: a highly efficient conjugated polymer for polymer solar cells with a regioregular structure†

Huifeng Yao,[a] Wenchao Zhao,[a] Zhong Zheng,[a] Yong Cui,[a] Jianqi Zhang,[b] Zhixiang Wei[b] and Jianhui Hou*[a]

Received 26th October 2015
Accepted 18th December 2015

DOI: 10.1039/c5ta08614k

www.rsc.org/MaterialsA

In this study, a regioregular copolymer (PBDT-TSR) based on alkythio-substituted two dimensional conjugated benzodithiophene (2D-BDT) and asymmetric thienothiophene (TT) was synthesized through two steps. Compared with its random counterpart PBDT-TS1, the PBDT-TSR shows improved absorption properties and enhanced inter-chain π–π packing effects. The hole mobility of PBDT-TSR is higher than that of PBDT-TS1. What's more, the enhancement of regioregularity does not have great influence on its molecular energy levels of the polymer and its miscibility with the acceptor material, $PC_{71}BM$. The polymer solar cell (PSC) device fabricated by using PBDT-TSR shows a high power conversion efficiency of 10.2% with a short-circuit current density (J_{SC}) of 17.99 mA cm^{-2}, while the PBDT-TS1 shows a PCE of 9.74%. Overall, these results suggest that it is of great importance to investigate the influence of backbone configuration on photovoltaic performance for high efficiency conjugated polymers based on asymmetric conjugated building blocks, and to improve the regioregularity of this type of polymer should be a feasible approach to enhance their photovoltaic properties.

Introduction

Organic semiconductors including conjugated polymers, oligomers and small molecules have been broadly used in electronic devices like organic light-emitting diodes (OLEDs), organic field-effect transistors (OFETs) and organic photovoltaic cells (OPVs).[1–7] In comparison with inorganic semiconductors, optoelectronic and electronic properties of organic semiconductors can be easily tuned by changing their molecular structures.[8–18] For example, absorption spectra, molecular energy levels and carrier mobilities of conjugated polymers can be effectively tuned by modulating their conjugated backbone or/and side groups. In fact, the electronic properties of organic semiconductors are so sensitive to their chemical structures that sometimes a subtle change in the molecular structure may have a significant effect on the device performance.

For conjugated small molecules and polymers, when asymmetric conjugated building blocks exist in their backbones, the relationship between the molecular structure and device performance becomes more complicated.[19–29] For instance, for the small molecular semiconductor in OFETs, the change of thiophene orientation in oligothiophene had a great effect on the film morphology, which resulted in different electron mobilities from 0.44 to 3.0 $cm^2\ V^{-1}\ s^{-1}$.[21] For conjugated polymers with asymmetric building blocks, the configuration of their backbones can also affect the properties of the devices. For example, the hole mobility of a regioregular pryidalthiadiazole based copolymer is two orders of magnitude higher than its counterpart with a random molecular structure.[30] Therefore, for molecular design of organic semiconductors, it is an important topic to investigate the influence of the configuration of asymmetric conjugated units on their optoelectronic properties.

For polymeric photovoltaic materials with asymmetric conjugated units, the change of backbone configurations will affect their optical and electronic properties and thus the photovoltaic performance. For example, as the regioregularity of P3HT increased, the absorption properties of the P3HT film could be improved, and the hole mobility had about one order magnitude enhancement.[20] As a result, a high power convention efficiency (PCE) of 4.4% was recorded for the polymer solar cell (PSC) devices based on P3HT with a regioregularity of 95.2% while the PCE was only 1.8% for the P3HT with a low regioregularity (90.7%).[19] Besides 3-alkylthiophene, quite a few asymmetric conjugated building blocks have been used in photovoltaic polymers, and the backbone configurations of the

[a]State Key Laboratory of Polymer Physics and Chemistry, Beijing National Laboratory for Molecular Sciences, Institute of Chemistry, Chinese Academy of Sciences, Beijing 100190, P. R. China. E-mail: hjhzlz@iccas.ac.cn; Tel: +86-10-82615900

[b]Key Laboratory of Nanosystem and Hierarchical Fabrication, National Center for Nanoscience and Technology, Beijing 100190, P. R. China

† Electronic supplementary information (ESI) available: Additional cyclic voltammetry and hole mobility measurement of the polymers. See DOI: 10.1039/c5ta08614k

polymers always affect their photovoltaic performance. For instance, compared with the random copolymer based on monofluorinated benzothiadiazole (FBT) and benzodithiophene (BDT), its regioregular analogue had improved intermolecular π–π interaction and enhanced hole mobility, which contributed to significant increase in short-circuit current density (J_{SC}) in the corresponding PSC devices, *i.e.* from 7.25 to 10.82 mA cm^{-2}, and hence the PCE increased to 5.92 from 3.91%.[23] Therefore, it is a useful method to improve photovoltaic properties of conjugated polymers with asymmetric building blocks by increasing the regioregularity of their conjugated backbones.

In recent years, the low band gap (LBG) conjugated polymers composed of BDT and thienothiophene (TT) units, such as PBDTTT-C-T,[31] PTB7,[32] and PTB7-Th,[33] demonstrated excellent photovoltaic properties and attracted broad attention of researchers. Since TT is an asymmetric unit in nature, different molecular configurations exist in all the PBDT–TT polymer family. Recently, Jen and coworkers found that there were two major isomers existing in the backbones of PBDT–TT polymers, and the content of the dominant isomer was 64%.[34] By controlling the orientation of TT, Lee *et al.* synthesized a regioregular PBDTTT-C-T, and the PCE of the PSC devices showed 19% improvement than its region-random counterpart. However, the PCE of the regioregular PBDTTT-C-T-based PSC was still lower than 8%.[35] Recently, our group developed a new polymer named as PBDT-TS1 comprising a linear alkythio modified 2D-conjugated BDT (2D-BDT) and TT, due to its superior absorption spectrum and molecular energy levels, the best PSC devices based on PBDT-TS1 showed an outstanding PCE near 10%.[36–39] In this work, we synthesized the regioregular derivative of this highly efficient photovoltaic polymer PBDT-TS1 (namely PBDT-TSR, as shown in Scheme 1) *via* a two-step method, and the detailed synthesis procedure is described in Scheme 2. The comparisons between the two polymers with the same chemical composition but different configurations revealed that the regioregular polymer, PBDT-TSR, has a stronger inter-chain aggregation effect in solution state, enhanced intermolecular π–π interactions and improved hole mobility in a solid thin film, and the PSC devices based on PBDT-TSR yielded higher PCE than PBDT-TS1.

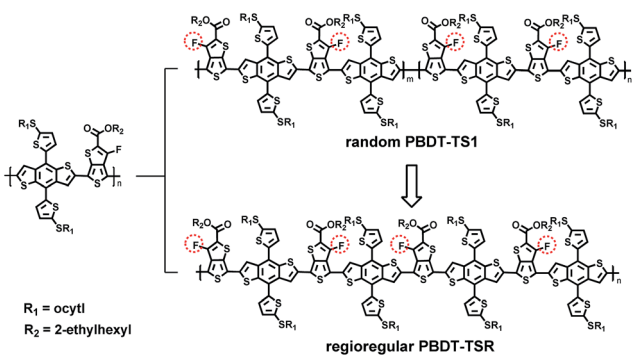

Scheme 1 Chemical structures of PBDT-TS1 and PBDT-TSR.

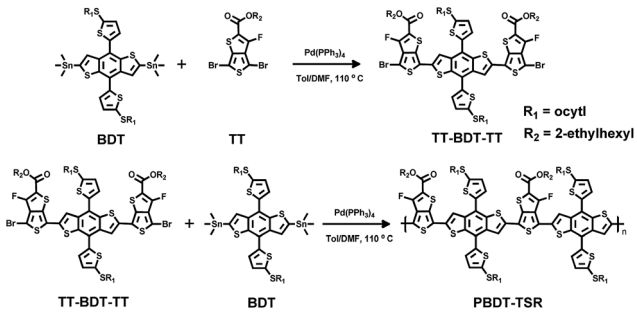

Scheme 2 Synthesis procedure of PBDT-TSR.

Results and discussion

Synthesis and thermal stability

Since the 4- and 6-positions of TT have different reactivity, the regioregular PBDT-TSR was synthesized through two steps as described in Scheme 2, which is similar to the reported work.[34] First, the intermediate TT–BDT–TT with one BDT unit and two oriented TT units was synthesized by adding the BDT solution into two equivalents of TT solution dropwise. Because the 6-position of TT had higher reactivity, the TT–BDT–TT unit with two fluorine atoms aside the BDT core would be the primary product. Then the PBDT-TSR was prepared by a conventional Stille coupling reaction. The detailed synthesis procedure is provided in the Experimental section. Gel permeation chromatography (GPC) was used to measure the molecular weight of the PBDT-TSR by using trichlorobenzene at 140 °C, and the result suggests a number-average molecular weight (M_n) of 30 kDa with a polydispersity index (PDI) of 2.1 for PBDT-TSR. As shown in Fig. 1, the thermal stability of the polymers PBDT-TS1 and PBDT-TSR was measured by thermogravimetric analysis (TGA). The PBDT-TSR shows a decomposition temperature of about 360 °C at 5% weight loss, which is slightly higher than that of PBDT-TS1. As provided in the ESI (see Fig. S1†), the electrochemical cyclic voltammetry (CV) measurements of the two polymer films show that they show the same p- and n-doping potentials, suggesting that the highest occupied molecular orbit (HOMO) and the lowest unoccupied molecular

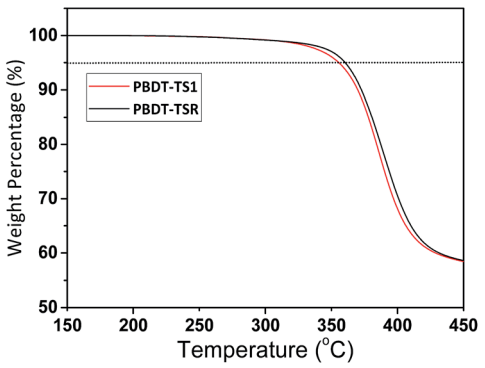

Fig. 1 TGA plots of the PBDT-TS1 and PBDT-TSR under the protection of nitrogen with a heating rate of 5 °C min^{-1}.

orbit (LUMO) of these two polymers are identical. Specially, the HOMO levels and LUMO levels of the two polymers are −5.30 and −3.45 eV, respectively.

Optical properties

As shown in Fig. 2a, PBDT-TS1 and PBDT-TSR in dilute chlorobenzene solution show different absorption features at varied temperatures (−20, 40 and 120 °C). For both the solutions, when the temperature is reduced, absorption intensity at 650–750 nm distinctly increases and an absorption peak located at *ca.* 745 nm emerges gradually, suggesting that the aggregation effect of the polymers in solution becomes stronger at low temperature. Notably, at the same temperature (as shown in Fig. S2†), the absorption intensity of PBDT-TSR in a long wavelength range is stronger than that of PBDT-TS1, implying that the regioregular polymer has stronger inter-chain interaction in the solution state than in the random polymer. Moreover, the absorption spectra of the two polymer films are demonstrated in Fig. 2b, from which we found that the main absorption peak of PBDT-TSR had a 5 nm red-shift compared to PBDT-TS1, and the extinction efficiency of PBDT-TSR is a little higher than that of PBDT-TS1. The different absorption features of PBDT-TSR and PBDT-TS1 suggest that the regioregular structure of PBDT-TSR contributes to a stronger inter-chain packing effect, and also the enhanced absorption of PBDT-TSR should be of benefit to harvest sunlight in PSCs.

Crystalline properties and hole mobility

Grazing-incidence wide-angle X-ray scattering (GIWAXS) was used to investigate the crystalline characteristics of the regioregular and random polymers. As presented in Fig. 3a and b, for both the two polymers, (010) diffraction peaks can be clearly observed in the out-of-plane direction, indicating that the polymers have a preferable face-on orientation in the film. In Fig. 3c, the (010) diffraction peaks of the two polymer films are located at the same position ($q = 1.69$ Å^{-1}), corresponding to a π–π stacking distance of 3.72 Å. It should be noted that the intensity of the (010) diffraction peak of PBDT-TSR is much stronger than that of PBDT-TS1. The in-plane diffraction profiles (see Fig. 3d) of the two polymers are quite similar. The UV-vis absorption features and GIWAXS results suggest that the PBDT-TSR has a stronger π–π stacking effect in the thin film than PBDT-TS1, which may be helpful for hole transport in the thin film. Therefore, we measured the hole mobilities of the polymers by the space-charge-limited current (SCLC) method,[40] and a hole-only device structure, ITO/PEDOT:PSS/polymer/Au, was employed in the measurement. Calculated from the plots shown in Fig. S3,† the hole mobility of regioregular PBDT-TSR is 3.16×10^{-2} cm^2 V^{-1} s^{-1}, which is about 3 times higher than its random analogue PBDT-TS1 (8.78×10^{-3} cm^2 V^{-1} s^{-1}).

Photovoltaic performance

To investigate the influence of molecular regioregularity on the photovoltaic performance, we fabricated the PSC with a conventional structure of ITO/PEDOT:PSS/polymer:$PC_{71}BM$/Mg/Al. The same processing conditions as reported in the work[36] were used in the preparation of the PBDT-TSR based devices, and the control devices based on PBDT-TS1 were also fabricated under the same conditions in parallel. Specifically, the mixture of the polymer and $PC_{71}BM$ (D/A ratio = 1 : 1.5) was dissolved in chlorobenzene (CB) solution (10 mg mL^{-1}, based on polymer weight concentration), and 3% (v/v) 1,8-diiodoctane

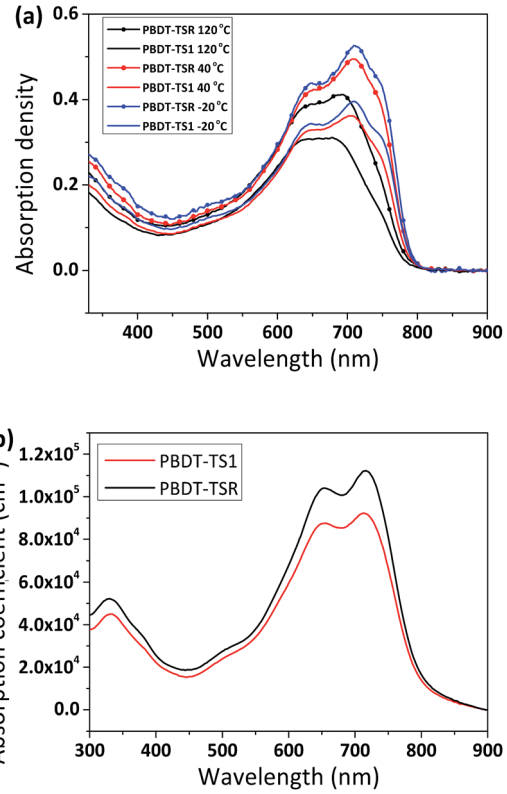

Fig. 2 (a) Absorption density of PBDT-TS1 and PBDT-TSR in dilute chlorobenzene solution (10^{-5} M) at varied temperatures, (b) film extinction efficiency of the two polymers.

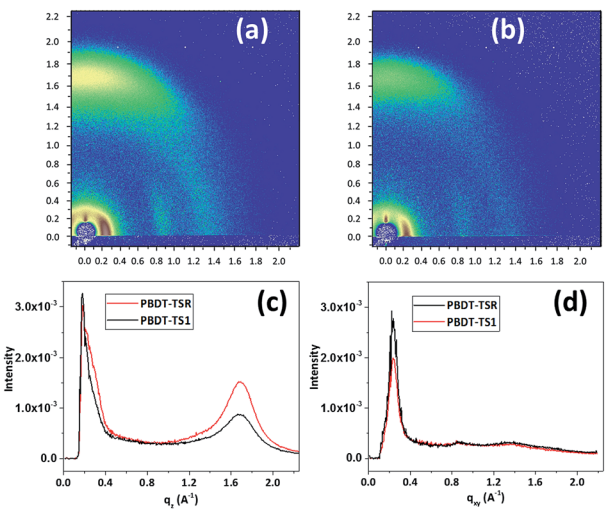

Fig. 3 2D GIWAXS patterns of the films for (a) PBDT-TSR and (b) PBDT-TS1, (c) out-of-plane images, and (d) in-plane images.

(DIO) was used as a solvent additive to optimize the morphology of the active layer; after spin-coating of *ca.* 100 nm active layer, 60 μL of menthol was spin-coated on the active layer to remove the residual additive. As shown in Fig. 4a, the current density–voltage (*J*–*V*) plots of the PSC devices were obtained under the illumination of AM 1.5G (100 mW cm^{-2}), and the detailed photovoltaic parameters are listed in Table 1. The open circuit voltage (V_{OC}) of the two types of devices are almost the same. From PBDT-TS1 to PBDT-TSR, J_{SC} of the corresponding device increases from 17.72 to 17.99 mA cm^{-2}, and the fill factor (FF) slightly improved from 68.57 to 70.55%. A high PCE of 10.20% is obtained for the PBDT-TSR-based devices while the PBDT-TS1-based device shows a PCE of 9.74% in parallel. The external quantum efficiency (EQE) of the devices was measured to confirm the enhancement of the J_{SC} for PBDT-TSR based devices. As demonstrated in Fig. 4b, the two devices show a similar response range while the PBDT-TSR-based device has a higher EQE value in the range of 450–750 nm, which should be caused by the improved absorption extinction coefficient of PBDT-TSR.

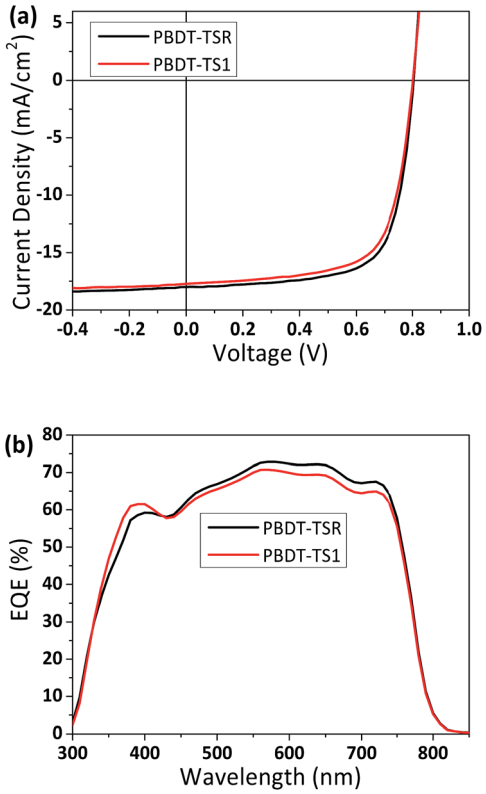

Fig. 4 (a) *J*–*V* curves and (b) EQE plots of the solar cell devices based on PBDT-TS1 and PBDT-TSR.

Table 1 Detailed photovoltaic parameters of PSC devices based on the PBDT-TS1 and PBDT-TSR

Polymers	V_{OC} (V)	J_{SC} (mA cm^{-2})	FF (%)	PCE[a] (%)	Thickness (nm)
PBDT-TS1	0.802	17.72	68.57	9.74 (9.52)	98
PBDT-TSR	0.804	17.99	70.55	10.20 (9.91)	106

[a] Average values of PCEs for thirty devices are shown in the brackets.

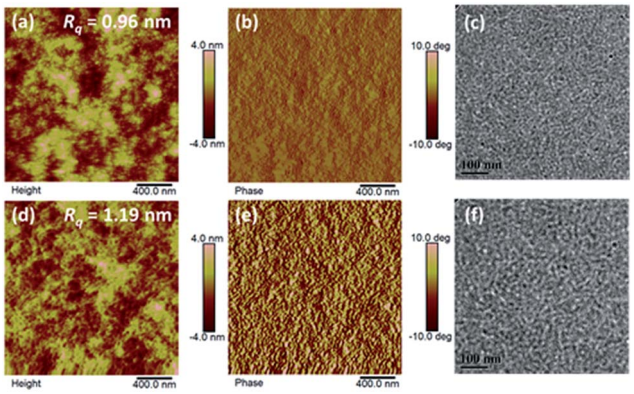

Fig. 5 Morphology images of polymer blends: (a) AFM height image, (b) AFM phase image, (c) TEM image of PBDT-TS1/$PC_{71}BM$, and (d) AFM height image, (e) AFM phase image, (f) TEM image of PBDT-TSR/$PC_{71}BM$.

Morphology study

Atomic force microscopy (AFM) and transmission electron microscopy (TEM) measurements were conducted to study the influence of regioregularity on phase separation features of the blend films processed by the optimal conditions for fabricating PSC devices. Fig. 5a and d show the AFM topographies of the two polymer blends, and the root mean square (RMS) roughness of the PBDT-TSR:$PC_{71}BM$ blend is 1.19 nm, which is slightly higher than that of the PBDT-TS1:$PC_{71}BM$ blend (0.96 nm). The AFM phase images are demonstrated in Fig. 5b and e. It can be observed that although the aggregation sizes in these two phase images are quite similar, the contrast of the two phases in the PBDT-TSR:$PC_{71}BM$ blend film is much higher than that in the PBDT-TS1:$PC_{71}BM$ blend film. In Fig. 5c and f, the TEM images of two blend films show similar nanoscale phase separation features, and appropriate domain sizes can be observed in both the films. According to the AFM and TEM measurements, we can conclude that compared to PBDT-TS1, PBDT-TSR can form stronger phase separation with $PC_{71}BM$ without affecting the aggregation size.

Conclusions

In conclusion, in order to improve photovoltaic property of PBDT-TS1, we synthesized the regioregular PBDT-TSR through two steps. In comparison with PBDT-TS1, the UV-vis absorption spectra results suggest that the PBDT-TSR has stronger inter-chain aggregation effect in the solution state and higher extinction coefficient in the solid thin film. The GIWASX measurements imply that the π–π stacking effect in PBDT-TSR film is stronger than that in PBDT-TS1 film. The hole mobility of PBDT-TSR reached 3.16 × 10^{-2} cm^2 V^{-1} s^{-1}, which is three times higher than PBDT-TS1. More importantly, the PBDT-TSR based PSC device yields a high PCE of 10.2% with a J_{SC} of 17.99

mA cm^{-2}. The results indicate that the backbone configuration in conjugated polymers with asymmetric building blocks has great impact on their optical, electronic properties and thus the photovoltaic performance, and improving the regioregularity of this type of polymer should be a feasible approach to enhance their photovoltaic properties.

Experimental

Materials and synthesis

PBDT-TS1 was prepared according the reported procedures.[36] The acceptor $PC_{71}BM$ and the monomer of BDT and TT were commercially available from Solarmer Material Inc. $Pd(PPh_3)_4$ was purchased from Frontiers Scientific Inc. and used as received.

Synthesis of TT–BDT–TT. TT (2.2 mmol, 1.038 g) monomer was dissolved in 30 mL of toluene and 3 mL of *N*,*N*-dimethylformamide (DMF) in the presence of $Pd(PPh_3)_4$ under an argon atmosphere, then the mixture was placed into a 100 °C oil bath. A solution of (1 mmol, 968 mg) BDT in 30 mL toluene was added slowly in 3 hours with the assistance of a peristaltic pump, then the reaction was stirred for other 5 hours. The solvent was removed by rotary evaporation. The target product was purified through silica gel column chromatography by using dichloromethane and petroleum ether as eluent. 570 mg (yield 40%) of TT–BDT–TT was obtained as a dark solid.

MS (MALDI-TOF) *m*/*z*: $[M]^+$ calcd for $C_{64}H_{74}Br_2F_2O_4S_{10}$: 1426; found 1426.

^{1}H NMR ($CDCl_3$, 400 MHz), δ (ppm): δ 7.87 (s, 2H), δ 7.36 (d, 2H), δ 7.23 (d, 2H), δ 4.26 (m, 4H), δ 2.97 (t, 4H), δ 1.74 (m, 6H), δ 1.30–1.48 (m, 40H), δ 0.90–1.25 (m, 18H).

^{13}C NMR ($CDCl_3$, 300 MHz), δ (ppm): 161.1, 151.5, 148.6, 141.3, 139.7, 138.0, 137.7, 137.2, 134.5, 133.1, 131.0, 130.8, 130.6, 129.0, 123.9, 123.4, 118.8, 100.6, 100.6, 68.4, 39.1, 32.1, 30.7, 29.7, 29.4, 29.2, 28.8, 24.2, 23.2, 22.9, 14.3, 11.3.

Elemental analysis calcd (%) for $C_{64}H_{74}Br_2F_2O_4S_{10}$: C 53.92, H 5.23. Found: C 53.97, H 5.29.

Synthesis of PBDT-TSR. 0.15 mmol of monomer TT–BDT–TT and equivalent monomer BDT was added into a 50 mL two necked flask, and 9 mL of toluene and 1.5 mL of DMF were added. The mixture was purged with argon for 5 min, and then 25 mg of catalyst ($Pd(PPh_3)_4$) was added. After being purged for another 15 minutes, the reaction was moved to 110 °C oil bath and stirred for 12 hours. The raw product was precipitated into methanol and filtered through a Buchner funnel. The solid was purified by Soxhlet extraction with methanol, hexanes, and chloroform, successively. The polymer was obtained from the chloroform fraction by precipitation from methanol. The dark solid was filtered and dried under vacuum for 24 hours.

Elemental analysis calcd (%) for $C_{49}H_{57}FO_2S_8$: C 61.72, H 6.03. Found: C 61.28, H 6.06.

Instruments and measurements

^{1}H NMR and ^{13}C NMR spectra were recorded on a Bruker AVANCE 400 MHz or a Frontier 300 MHz spectrometer at room temperature. Absorption spectra of polymers in solution at varied temperatures and solid thin films were recorded on a Hitachi UH4150 UV-Vis spectrophotometer. The CV measurements were recorded on a CHI650D Electrochemical Workstation, and the glassy carbon, platinum wire, and Ag/Ag^+ electrode were used as the working electrode, counter electrode and reference electrode respectively. 0.1 M tetrabutylammonium hexafluorophosphate (Bu_4NPF_6) acetonitrile solution was used as the electrolyte. Elemental analysis data were recorded on a flash EA1112 analyzer. The GIWAXS data were obtained on a XEUSS SAXS/WAXS SYSTEM (XENOCS, FRANCE) at the National Center for Nanoscience and Technology (NCNST, Beijing). According to our previous work,[41] the *J*–*V* characteristics were measured under the 100 mW cm^{-2} standard AM 1.5G spectrum through a Class AAA solar simulator, and a NIM calibrated KG3-filtered cell was used as the reference cell. An integrated IPCE system named QE-R3011 (Enli Technology Co. Ltd., Taiwan) was used to obtain the EQE spectra. The AFM patterns were recorded by using a Nanoscope V AFM in the tapping mode. The TEM patterns were recorded on a JEOL 2200FS instrument by using 160 kV accelerating voltage in the bright field mode.

Fabrication of the PSC devices

The PSC devices were fabricated through our reported work, and they have the structure of ITO/PEDOT:PSS/polymer:PC_{71}BM/Mg/Al. The fabrication processes were performed under the following procedures: ITO glasses were cleaned by using the surfactant scrub, washed with water, acetone and isopropanol, successively. Then UV-ozone treatment was performed on the ITO surface for 15 minutes. About 35 nm thick of PEDOT:PSS was spin-coated on the ITO glasses, and the ITO substrates were dried in an oven at 150 °C for 15 min. The solution of polymer/PC_{71}BM (10 mg mL^{-1}, based on the polymer weight concentration) in chlorobenzene was spin-coated on the PEDOT:PSS layer. Then a small amount of methanol was spin-coated on the active layer to remove the residual additives.[42] Under high vacuum, about 20 nm of Mg and 80 nm of Al were deposited onto the active layer successively, giving an effective cell area of 4.15 mm^2. Except for the spin-coating of PEDOT:PSS, the other processes were carried out in a glovebox of nitrogen atmosphere.

Acknowledgements

We gratefully acknowledge the financial support from Ministry of Science and Technology of China (2014CB643501), NSFC (21325419, 51373181, 91333204), the Chinese Academy of Science (XDB12030200, KJZD-EW-J01).

Notes and references

1 C. W. Tang and S. A. Vanslyke, *Appl. Phys. Lett.*, 1987, **51**, 913.
2 A. Facchetti, *Chem. Mater.*, 2011, **23**, 733.
3 G. Li, R. Zhu and Y. Yang, *Nat. Photonics*, 2012, **6**, 153.

4 T. W. Kelley, P. F. Baude, C. Gerlach, D. E. Ender, D. Muyres, M. A. Haase, D. E. Vogel and S. D. Theiss, *Chem. Mater.*, 2004, **16**, 4413.
5 S. Günes, H. Neugebauer and N. S. Sariciftci, *Chem. Rev.*, 2007, **107**, 1324.
6 L. Lu, T. Zheng, Q. Wu, A. M. Schneider, D. Zhao and L. Yu, *Chem. Rev.*, 2015, **115**, 12666.
7 L. Dou, Y. Liu, Z. Hong, G. Li and Y. Yang, *Chem. Rev.*, 2015, **115**, 12633.
8 J. H. Hou, M. H. Park, S. Q. Zhang, Y. Yao, L. M. Chen, J. H. Li and Y. Yang, *Macromolecules*, 2008, **41**, 6012.
9 J. Chen and Y. Cao, *Acc. Chem. Res.*, 2009, **42**, 1709.
10 Y. J. Cheng, S. H. Yang and C. S. Hsu, *Chem. Rev.*, 2009, **109**, 5868.
11 P. M. Beaujuge and J. M. J. Fréchet, *J. Am. Chem. Soc.*, 2011, **133**, 20009.
12 H. Yao, L. Ye, B. Fan, L. Huo and J. Hou, *Science China Materials*, 2015, **58**, 213.
13 C. Duan, F. Huang and Y. Cao, *J. Mater. Chem.*, 2012, **22**, 10416.
14 Z. B. Henson, K. Mullen and G. C. Bazan, *Nat. Chem.*, 2012, **4**, 699.
15 H. Yao, H. Zhang, L. Ye, W. Zhao, S. Zhang and J. Hou, *ACS Appl. Mater. Interfaces*, 2015, DOI: 10.1021/acsami.5b07311.
16 Y. F. Li, *Acc. Chem. Res.*, 2012, **45**, 723.
17 L. Ye, S. Zhang, L. Huo, M. Zhang and J. Hou, *Acc. Chem. Res.*, 2014, **47**, 1595.
18 H. F. Yao, H. Zhang, L. Ye, W. C. Zhao, S. Q. Zhang and J. H. Hou, *Macromolecules*, 2015, **48**, 3493.
19 Y. Kim, S. Cook, S. M. Tuladhar, S. A. Choulis, J. Nelson, J. R. Durrant, D. D. C. Bradley, M. Giles, I. McCulloch, C.-S. Ha and M. Ree, *Nat. Mater.*, 2006, **5**, 197.
20 C. H. Woo, B. C. Thompson, B. J. Kim, M. F. Toney and J. M. J. Fréchet, *J. Am. Chem. Soc.*, 2008, **130**, 16324.
21 C. Zhang, Y. Zang, E. Gann, C. R. McNeill, X. Zhu, C.-a. Di and D. Zhu, *J. Am. Chem. Soc.*, 2014, **136**, 16176.
22 C. Zhang, H. Li, J. Wang, Y. Zhang, Y. Qiao, D. Huang, C.-a. Di, X. Zhan, X. Zhu and D. Zhu, *J. Mater. Chem. A*, 2015, **3**, 11194.
23 T. Qin, W. Zajaczkowski, W. Pisula, M. Baumgarten, M. Chen, M. Gao, G. Wilson, C. D. Easton, K. Müllen and S. E. Watkins, *J. Am. Chem. Soc.*, 2014, **136**, 6049.
24 Q. Peng, X. Liu, D. Su, G. Fu, J. Xu and L. Dai, *Adv. Mater.*, 2011, **23**, 4554.
25 Y. Li, Z. Pan, L. Miao, Y. Xing, C. Li and Y. Chen, *Polym. Chem.*, 2014, **5**, 330.
26 H. Zhou, L. Yang, S. C. Price, K. J. Knight and W. You, *Angew. Chem., Int. Ed.*, 2010, **49**, 7992.
27 L. Ying, B. B. Y. Hsu, H. Zhan, G. C. Welch, P. Zalar, L. A. Perez, E. J. Kramer, T.-Q. Nguyen, A. J. Heeger, W.-Y. Wong and G. C. Bazan, *J. Am. Chem. Soc.*, 2011, **133**, 18538.
28 G. C. Welch, R. C. Bakus II, S. J. Teat and G. C. Bazan, *J. Am. Chem. Soc.*, 2013, **135**, 2298.
29 M. Wang, H. Wang, T. Yokoyama, X. Liu, Y. Huang, Y. Zhang, T. Q. Nguyen, S. Aramaki and G. C. Bazan, *J. Am. Chem. Soc.*, 2014, **136**, 12576.
30 Z. B. Henson, G. C. Welch, T. van der Poll and G. C. Bazan, *J. Am. Chem. Soc.*, 2012, **134**, 3766.
31 L. Huo, S. Zhang, X. Guo, F. Xu, Y. Li and J. Hou, *Angew. Chem., Int. Ed.*, 2011, **50**, 9697.
32 Y. Liang, Z. Xu, J. Xia, S.-T. Tsai, Y. Wu, G. Li, C. Ray and L. Yu, *Adv. Mater.*, 2010, **22**, E135.
33 S.-H. Liao, H.-J. Jhuo, Y.-S. Cheng and S.-A. Chen, *Adv. Mater.*, 2013, **25**, 4766.
34 H. Zhong, C.-Z. Li, J. Carpenter, H. Ade and A. K. Y. Jen, *J. Am. Chem. Soc.*, 2015, **137**, 7616.
35 H. Kim, H. Lee, D. Seo, Y. Jeong, K. Cho, J. Lee and Y. Lee, *Chem. Mater.*, 2015, **27**, 3102.
36 L. Ye, S. Zhang, W. Zhao, H. Yao and J. Hou, *Chem. Mater.*, 2014, **26**, 3603.
37 S. Q. Zhang, L. Ye, W. C. Zhao, B. Yang, Q. Wang and J. H. Hou, *Sci. China: Chem.*, 2015, **58**, 248.
38 S. Zhang, M. A. Uddin, W. Zhao, L. Ye, H. Y. Woo, D. Liu, B. Yang, H. Yao, Y. Cui and J. Hou, *Polym. Chem.*, 2015, **6**, 2752.
39 J. Liu, X. Li, S. Zhang, X. Ren, J. Cheng, L. Zhu, D. Zhang, L. Huo, J. Hou and W. C. H. Choy, *Adv. Mater. Interfaces*, 2015, DOI: 10.1002/admi.201500324.
40 A. Rose, *Phys. Rev.*, 1955, **97**, 1538.
41 L. Ye, C. Zhou, H. Meng, H.-H. Wu, C.-C. Lin, H.-H. Liao, S. Zhang and J. Hou, *J. Mater. Chem. C*, 2015, **3**, 564.
42 L. Ye, Y. Jing, X. Guo, H. Sun, S. Zhang, M. Zhang, L. Huo and J. Hou, *J. Phys. Chem. C*, 2013, **117**, 14920.